

CaDA: Cross-Problem Routing Solver with Constraint-Aware Dual-Attention

1st Han Li

*School of System Design and
Intelligent Manufacturing
Southern University of
Science and Technology
Shenzhen, China
herloconnell@gmail.com*

2nd Fei Liu

*Department of Computer Science
City University of Hong Kong
Hong Kong, China
fliu36-c@my.cityu.edu.hk*

3rd Zhi Zheng

*School of System Design and
Intelligent Manufacturing
Southern University of
Science and Technology
Shenzhen, China
12010126@mail.sustech.edu.cn*

4th Yu Zhang

*School of System Design and Intelligent Manufacturing
Southern University of Science and Technology
Shenzhen, China
zhangy5@sustech.edu.cn*

5th Zhenkun Wang

*School of System Design and Intelligent Manufacturing
Southern University of Science and Technology
Shenzhen, China
wangzhenkun90@gmail.com*

Abstract—Vehicle Routing Problems (VRPs) are significant Combinatorial Optimization (CO) problems holding substantial practical importance. Recently, Neural Combinatorial Optimization (NCO), which involves training deep learning models on extensive data to learn vehicle routing heuristics, has emerged as a promising approach due to its efficiency and the reduced need for manual algorithm design. However, applying NCO across diverse real-world scenarios with various constraints necessitates cross-problem capabilities. Current multi-task methods for VRPs typically employ a constraint-unaware model, limiting their cross-problem performance. Furthermore, they rely solely on global connectivity, which fails to focus on key nodes and leads to inefficient representation learning. This paper introduces a Constraint-Aware Dual-Attention Model (CaDA), designed to address these limitations. CaDA incorporates a constraint prompt that efficiently represents different problem variants. Additionally, it features a dual-attention mechanism with a global branch for capturing broader graph-wide information and a sparse branch that selectively focuses on the most relevant nodes. We comprehensively evaluate our model on 16 different VRPs and compare its performance against existing cross-problem VRP solvers. CaDA achieves state-of-the-art results across all the VRPs. Our ablation study further confirms that each component of CaDA contributes positively to its cross-problem learning performance.

Index Terms—Vehicle Routing Problem, Constraint-Aware Learning, Dual-Attention Mechanism, Cross-Problem Learning.

I. INTRODUCTION

Vehicle Routing Problems (VRPs) involve optimizing transportation costs for a fleet of vehicles to meet all customers' demands while adhering to various constraints. Numerous studies have focused on VRPs due to their extensive real-world applications in transportation, logistics, and manufacturing [1], [2]. Traditional methods for solving VRPs include exact solvers and heuristic methods. Exact solvers, however,

struggle with the NP-hard nature of the problem, making them prohibitively expensive to implement. On the other hand, heuristic methods are more cost-effective and provide near-optimal solutions but require significant expert input in their design. Recently, learning-based neural solvers have gained considerable attention and have been successfully applied to VRPs [3]–[5]. These solvers train networks to learn a heuristic, reducing the need for extensive manual algorithm design and minimizing computational overhead.

Despite the promising performance of neural solvers on VRPs, the majority of existing works require training a distinct model for each type of routing problem [6]–[13]. Given that over 60 VRP variants have been studied, each featuring different constraints [14], developing distinct models for each routing problem is costly and significantly hinders practical application.

To tackle this challenge, recent efforts have been made to develop cross-problem learning methods that can solve multiple VRPs with a single model [15]–[18]. These cross-problem methods typically employ an encoder-decoder framework and are trained using reinforcement learning. For example, MTPOMO [15] jointly trains a unified model across five VRPs, each with one or two constraints, enabling zero-shot generalization to problems that feature combinations of these constraints. MVMoE [16] employs a Mixture-of-Experts (MoE) [19] structure in the feed-forward layer of a transformer-based model to enhance its cross-problem learning capacity. Furthermore, RouteFinder [17] directly trains and tests sixteen VRPs using a proposed unified Reinforcement Learning (RL) environment, which enables the simultaneous handling of different VRPs in the same training batch. Additionally, RouteFinder leverages a modern transformer-based model structure [20], along with global embeddings,

to enhance performance.

Despite these advancements, existing cross-problem models remain unaware of constraints [15]–[17]. As different constraints significantly alter the feasible solution space, this oversight notably limits the models’ capabilities in cross-problem applications. Furthermore, existing methods employ a transformer encoder which maintains global connectivity throughout the node encoding process, leading to the inclusion of irrelevant nodes and adversely affecting node representation. Conversely, using learnable sparse connections [21], [22] allows the node encoding process to selectively focus on more relevant nodes.

This study proposes a novel Constraint-Aware Dual-Attention Model (CaDA) to mitigate these challenges. Firstly, we introduce a constraint prompt to enhance the model’s awareness of the activated constraints. Furthermore, we propose a dual-attention mechanism consisting of a global branch and a sparse branch. Since, in the encoder-decoder framework, node pairs with higher attention scores are more likely to be adjacent in the solution, the sparse branch with Top- k sparse attention focuses on the more promising connections between these key node pairs. Meanwhile, the global branch enhances the model’s capacity by capturing information from the entire graph, ensuring that the solution is informed globally. The effectiveness and superiority of CaDA have been comprehensively demonstrated across 16 VRPs and real-world benchmarks.

The contributions of this paper can be summarized as follows:

- We introduce CaDA, an efficient cross-problem learning method for VRPs that enhances model awareness of constraints and representation learning.
- We propose a constraint prompt, which facilitates high-quality constraint-aware learning, and a dual-attention mechanism, which ensures that the encoding process is both selectively focused and globally informed.
- We conduct a comprehensive evaluation of CaDA across 16 VRP variants. CaDA achieves state-of-the-art performance, surpassing existing cross-problem learning methods. Additionally, our ablation study validates the effectiveness of both the constraint prompt and the dual-attention mechanism.

II. RELATED WORK

A. Neural Combinatorial Optimization

NCO approaches utilize deep reinforcement learning to train a policy that constructs solutions in an autoregressive manner. Nazari et al. [23] are the first to apply Pointer Networks [24] to solve the VRP. Subsequently, the pioneering work Attention Model (AM) [4] employs a powerful Transformer-based architecture. This model is optimized using the REINFORCE algorithm [25] with a greedy rollout baseline. Building on this, Kwon et al. [6] introduce the Policy Optimization with Multiple Optima (POMO) method, which leverages solution symmetries and has demonstrated significantly improved performance. Subsequently, numerous studies have further refined

both AM and POMO, enhancing Transformer-based methods [26]–[29]. Given the diverse constraints and attributes in real-world transportation needs, some research focuses on various VRP variants, including heterogeneous Capacitated VRP (HCVRP) [30], VRP with Time Windows (VRPTW) [9]–[12], and Open Route VRP (OVRP) [13]. More information can be found in recent reviews [31], [32].

B. Cross-Problem Learning for VRPs

Neural methods for solving VRPs typically train and evaluate deep models on the same instance distributions. Some studies have explored generalization across multiple distributions [33]–[38]. Additionally, Zhou et al. [39] consider both problem size and distribution variations. Recent developments have begun to address cross-problem generalization [15], [16], [18], [40]. Wang and Yu [40] use multi-armed bandits to achieve task scheduling. Lin et al. [18] demonstrate how a model pre-trained on the Travelling Salesman Problem (TSP) could be effectively adapted to targeted VRPs through efficient fine-tuning, e.g., inside tuning, side tuning, and Low-Rank Adaptation (LoRA). However, these approaches still focus on relatively few tasks (less than five).

To tackle multiple VRP variants in a unified model, MT-POMO [15] conceptualizes VRP variants as combinations of underlying constraints, enabling the model to achieve zero-shot generalizability to more tasks. MVMoE proposes a new model architecture using the MoE [19] approach to improve performance. Furthermore, RouteFinder [17] proposes to use a modern transformer encoder structure incorporating SwiGLU [41], Root Mean Square Normalization (RMSNorm) [42], and Pre-Norm [43], [44], which considerably improves the model’s capability. However, these approaches remain unaware of constraints and maintain only global connectivity throughout the encoding process, which limits their cross-problem capabilities.

C. Multi-Branch Architecture

Multi-branch architectures have been widely used and have achieved success in computer vision. Some research employs multiple branches to capture both low and high-resolution image information, ultimately producing a comprehensive and powerful semantic representation that can be used for downstream tasks such as image segmentation [45]–[47] or human pose estimation [48], [49]. Other studies assign different branches to focus on distinct aspects by utilizing attention mechanisms [50]–[53]. For instance, DANet [50] proposes a dual attention network for scene segmentation, with one branch responsible for capturing pixel-to-pixel dependencies and another for capturing channel dependencies across different feature maps, thereby capturing global context [54]. Similarly, Crossformer++ [53] groups image patches in both local and global ways, incorporating short-distance and long-distance attention to achieve better representation, retaining both small-scale and large-scale features in the embeddings. In this study, we propose a novel dual-attention mechanism featuring a global branch for capturing information from the

III. PRELIMINARIES

A. Problem Definition

In this study, we focus on 16 VRP variants that encompass five different constraints, including Capacity (C), Open Route (O), Backhaul (B), Duration Limit (L), and Time Window (TW). These are summarized in Table I, with illustrations related to these constraints presented in Figure 1. In this section, we begin by outlining a general definition of the VRP instance, then continue with the basic CVRP, and proceed to describe its four additional constraints.

A VRP instance \mathcal{G} is a fully-connected graph defined by a set of nodes $\mathcal{V} = \{v_0, v_1, \dots, v_N\}$ with the total number of nodes given by $|\mathcal{V}| = N + 1$, and edges $\mathcal{E} = \mathcal{V} \times \mathcal{V}$. Furthermore, v_0 represents the depot, while $\{v_1, \dots, v_N\}$ represent the N customer nodes. Each node $v_i \in \mathcal{V}$ consists of the pair $\{\vec{X}_i, A_i\}$, where $\vec{X}_i \sim U(0, 1)^2$ represents the node coordinates, and A_i denotes other attributes of the nodes. Additionally, the travel cost between different nodes is defined by their Euclidean distance, which is denoted by the cost matrix $\mathbf{D} = \{d_{i,j}, i = 0, \dots, N, j = 0 \dots, N\}$.

In CVRP, the depot node v_0 has $A_0 = \emptyset$, and each customer node v_i is associated with $A_i = \{\delta_i\}$, where δ_i is the customer's demand v_i that the fleet of vehicles must service. This fleet comprises homogeneous vehicles, each with a specific capacity C . Each vehicle leaves the depot v_0 , visits a subset of customers, and returns to the depot upon completion of deliveries. The solution to CVRP, denoted by τ , consists of the routes taken by all vehicles, that is, $\tau = \{\tau^1, \tau^2, \dots, \tau^K\}$, where K is the total number of sub-routes. Each sub-route $\tau^k = (\tau_1^k, \tau_2^k, \dots, \tau_{n_k}^k)$, $k \in 1, 2, \dots, K$, where τ_i^k is the index of the visited node at step i , and $\tau_1^k = \tau_{n_k}^k = 0$. $n_k = |\tau^k|$ represents the number of nodes in it, and $\sum_{k=1}^K n_k = T$ represents the total length of the solution.

The basic CVRP could be easily extended to accommodate various VRPs by incorporating additional constraints. In this paper, we explore four additional constraints as discussed in recent studies [15]–[17].

a) *Open Route (O)*: In the OVRP, vehicles do not return to the depot v_0 after completing their sub-route.

b) *Time Window (TW)*: The Time Window constraint requires that each node must be visited within a specific time window, such that each node $A_i = \{\delta_i, e_i, l_i, s_i\}$, where e_i is the earliest start time, l_i is the latest permissible time, and s_i represents the time taken to service this customer. The depot v_0 has $s_0 = 0$, $e_0 = 0$, and $l_0 = \mathcal{T}$, indicating that each sub-tour must be completed within a time limit of \mathcal{T} . Time window constraints are stringent; if a vehicle arrives earlier than e_i , it must wait until the start of the window.

c) *Backhaul (B)*: Customers with $\delta_i > 0$ are termed linehaul customers, as they require vehicles to load goods at the depot and deliver to their locations. Conversely, customers with $\delta_i < 0$ are defined as backhaul customers, where vehicles must collect $|\delta_i|$ from their locations and transport it back to the depot. While all customers in the standard CVRP are linehaul, the Vehicle Routing Problem With Backhauls (VRPB)

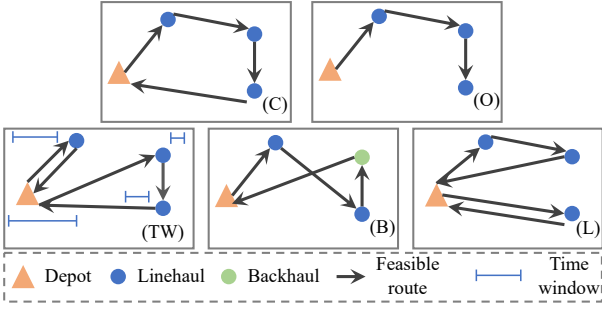


Fig. 1. The feasible solutions for different VRP variants.

TABLE I
16 VRP VARIANTS WITH FIVE CONSTRAINTS.

	Capacity	Open Route	Backhaul	Duration Limit	Time Window
CVRP	✓				
OVRP		✓			
VRPB	✓		✓		
VRPL	✓			✓	
VRPTW	✓				✓
OVRPTW	✓				✓
OVRPB	✓	✓	✓		
OVRPL	✓	✓		✓	
VRPBL	✓		✓	✓	
VRPBTW	✓		✓		✓
VRPLTW	✓			✓	✓
OVRPBL	✓	✓	✓	✓	
OVRPBTW	✓	✓	✓		✓
OVRPLTW	✓	✓		✓	✓
VRPBLTW	✓		✓	✓	✓
OVRPBLTW	✓	✓	✓	✓	✓

entire graph and a sparse branch to focus more on important connections.

D. Sparse Attention

Recent studies have proposed using sparse attention to reduce computational complexity and minimize the harmful influence of unnecessary and irrelevant items, thereby improving performance [21], [55]–[58]. To achieve this, many researchers utilize pre-defined sparse attention patterns based on prior knowledge, such as local or strided attention, or combinations of multiple patterns [59]–[62]. For instance, LogSparse [60] ensured that each token only attends to itself and its preceding tokens, using an exponential step size. However, these methods can be overly harsh and require well-informed prior knowledge. Another category of methods achieves sparse attention by adding an additive operation that eliminates small attention scores to exactly zero, such as the Top- k operation [21], [55]–[57] and the ReLU² operation [22], or employs a sparsity-inducing alternative to Softmax, such as sparsemax [63] and α -entmax [64]–[66]. In this study, we use the simple yet efficient Top- k selection operation to achieve sparse attention and enhance the representation learning from the most relevant nodes.

includes both linehaul and backhaul customers. Furthermore, all linehaul tasks must be completed before any backhaul tasks can commence on the route to avoid rearranging the loads on the vehicle.

d) Duration Limit (L): In this constraint, the depot v_0 has $A_0 = \{\rho\}$, where ρ represents the length limit that each sub-tour must adhere to, ensuring a return to v_0 within this threshold.

B. Learning to Construct Solutions for VRPs

The process of constructing solutions autoregressively (i.e., during decoding) can be modeled as a Markov Decision Process (MDP), and the policy can be trained using RL methods. As the model sequentially expands each sub-route, for simplicity, at any decoding step t , τ_t represents the sequence of nodes visited up to that point:

$$\tau_t = \bigcup_{k=1}^K (\tau_1^k, \tau_2^k, \dots, \tau_{n_k}^k) = (\tau_1, \tau_2, \dots, \tau_t), \quad (1)$$

where \bigcup denotes the concatenation of sequences from different sub-routes. The MDP for the decoding step t can be defined as follows:

a) State: $s_t \in \mathcal{S}$ is the ordered tuple $(\tau_{t-1}, \mathcal{V})$ given by the current partial solution $\tau_{t-1} = (\tau_1, \tau_2, \dots, \tau_{t-1})$ and the instance \mathcal{V} . Initially, $\tau_0 = \emptyset$, and at the end, s_T contains a feasible solution τ_T .

b) Action: $a_t \in \mathcal{A}$ is the selected index in the current step, which will be added at the end of the partial solution. If $a_t = 0$, i.e., the vehicle returns to the depot node, it signifies the end of the current sub-tour and the start of a new one.

c) Policy: A neural model π_θ with learnable parameters θ is used as a policy to generate solutions sequentially, where the probability of generating the final feasible solution is:

$$\pi_\theta(\tau | \mathcal{V}) = \prod_{t=1}^T \pi_\theta(a_t | s_t) = \prod_{t=1}^T \pi_\theta(\tau_t | \tau_{t-1}, \mathcal{V}). \quad (2)$$

d) Reward: $r \in \mathcal{R}$ can only be obtained when a whole feasible solution τ_T is generated and is defined as the negative solution length:

$$r(\tau_T) = - \sum_{t=1}^{T-1} d_{\tau_t \tau_{t+1}}. \quad (3)$$

Subsequently, π_θ can be optimized using RL methods to maximize the expected reward J . This study employs the REINFORCE algorithm [25] with a shared baseline proposed by Kwon et al. [6], to update the policy. Specifically, for a VRP instance \mathcal{V} , N trajectories are generated, starting with the first action $\{a_1^1, a_1^2, \dots, a_1^N\}$, which is always 0. Each of the N trajectories then assigns a unique one of the N customer nodes as the second point, i.e., $\{a_2^1, a_2^2, \dots, a_2^N\} = \{1, 2, \dots, N\}$. The policy subsequently samples actions for each trajectory

until all have derived feasible solutions $\{\tau^1, \tau^2, \dots, \tau^N\}$. Finally, the gradient of the policy is approximated by:

$$\begin{aligned} \nabla_\theta J(\theta | \mathcal{V}) &\approx \frac{1}{N} \sum_{i=1}^N (r(\tau^i) - b^i(\mathcal{V})) \nabla_\theta \log \pi_\theta(\tau^i | \mathcal{V}), \\ b^i(\mathcal{V}) &= \frac{1}{N} \sum_{j=1}^N r(\tau^j) \quad \text{for all } i. \end{aligned} \quad (4)$$

Where $b(\mathcal{V})$ is the shared baseline function used to stabilize learning.

For the structure of policy π_θ , existing approaches primarily use transformer-based models.

C. Transformer Layer

The Transformer [67] comprises a Multi-Head Attention Layer (MHA) and a Feed-Forward Layer (FFD). In some modern large language models [68]–[70], the FFD is replaced by Gated Linear Units (GLUs).

a) Attention Layer: The classical attention function can be expressed as:

$$\begin{aligned} \text{Attention}(X, Y) &= \mathbf{A}(YW_V), \\ \text{where } \mathbf{A} &= \text{Softmax}\left(\frac{XW_Q(YW_K)^\top}{\sqrt{d_k}}\right), \end{aligned} \quad (5)$$

where $X \in \mathbb{R}^{n \times d}$ and $Y \in \mathbb{R}^{m \times d}$ represent the input embeddings. The parameters $W_Q, W_K \in \mathbb{R}^{d \times d_k}$, and $W_V \in \mathbb{R}^{d \times d_v}$ are trainable matrices for the query, key, and value projections, respectively. After calculating the attention matrix using the query and key matrices, the Softmax function is applied independently across each row to normalize the attention scores. These scores are then rescaled by $\sqrt{d_k}$, resulting in the scaled attention score matrix \mathbf{A} . The eventual output, denoted as Z , is a matrix in $\mathbb{R}^{n \times d_v}$.

Additionally, for efficiency, the MHA projects X into M_h separate sets of queries, keys, and values, upon which the attention function is applied:

$$\begin{aligned} \text{MHA}(X, Y) &= \text{Concat}(Z_1, \dots, Z_{M_h})W_p, \\ \text{where } Z_i &= \text{Attention}_i(X, Y), \forall i \in \{1, \dots, M_h\}, \end{aligned} \quad (6)$$

where $d_k = d_v = \frac{d}{M_h}$ in each Attention_i . The parameter $W_p \in \mathbb{R}^{d \times d}$ denotes a trainable matrix combining different attention heads' outputs. For self-attention, we have $Y = X$.

b) Gated Linear Unit: The transformer blocks also include an FFD that processes the input X through two learned linear projections, with a ReLU activation function applied between them. In many recent modern transformer-based large language models [68]–[70], this configuration has been replaced by GLUs [41]. GLUs consist of a component-wise product of two linear projections, where one projection is first passed through a nonlinear function. We employ SwishGLU [41], which utilizes the Sigmoid Linear Unit (SiLU) [71] as the nonlinear function, as recommended in the RouteFinder [17]. The SwiGLU is defined as:

$$\text{SwiGLU}(X) = X \odot \sigma(XW_1 + b_1) \otimes \text{SiLU}(XW_2 + b_2). \quad (7)$$

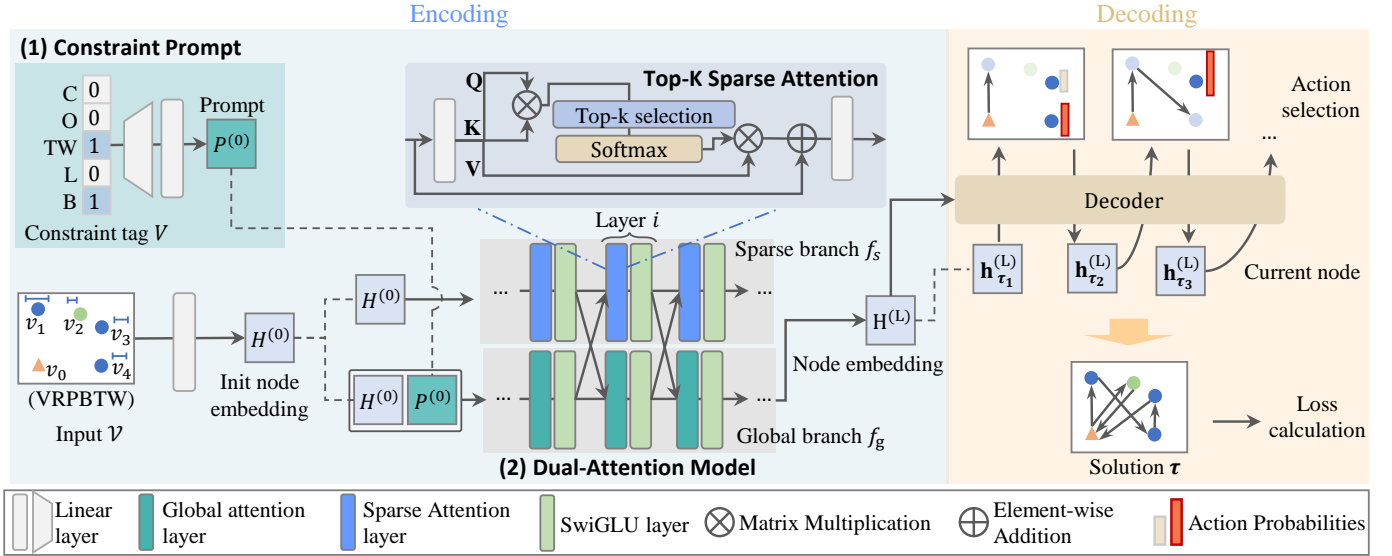


Fig. 2. The pipeline of the proposed CaDA for VRPs. CaDA adopts the typical encoder-decoder framework and incorporates two new components in the encoder: a dual-attention mechanism and a constraint prompt. The dual-attention mechanism comprises a global branch with the standard Softmax function and a sparse branch with Top- k operation.

where \odot denotes element-wise multiplication, \otimes is matrix multiplication, σ is the sigmoid function, and W_1, W_2, b_1, b_2 are learnable parameters.

IV. METHODOLOGY

A. Overall Pipeline

As shown in Figure 2, CaDA follows the general cross-problem learning framework for VRPs which consists of two stages: encoding instance \mathcal{V} to node embeddings $H^{(L)}$, and decoding to construct solutions based on $H^{(L)}$ sequentially. CaDA employs a prompt to introduce constraint information during the encoding process and further utilizes a dual-attention mechanism to enhance representation learning.

B. Constraint Prompt

To generate prompts that carry the problem's constraint information, we represent the problem as a multi-hot vector $V \in \mathbb{R}^5$, corresponding to five distinct constraints. This multi-hot vector is subsequently processed through a straightforward Multi-Layer Perceptron (MLP) to generate the prompts:

$$P^{(0)} = \text{LayerNorm}(VW_a + b_a)W_b + b_b, \quad (8)$$

where $W_a \in \mathbb{R}^{5 \times d_h}$, $b_a \in \mathbb{R}^{d_h}$, $W_b \in \mathbb{R}^{d_h \times d_h}$, and $b_b \in \mathbb{R}^{d_h}$ are learnable parameters. d_h is the node's embedding dimension. Then this prompt can be concatenated with the node embeddings.

C. Dual-Attention Mechanism

The input instance \mathcal{V} with $|\mathcal{V}| = N + 1$, is first transformed into high-dimensional initial node embeddings a linear projection. The initial node embedding is denoted as $H^{(0)} \in \mathbb{R}^{(N+1) \times d_h}$.

Subsequently, $H^{(0)}$ is concatenated with $P^{(0)}$ and processed through a global branch f_g , which consist of L layers. Each

consists of a standard MHA layer [67] and a SwiGLU [72]. The standard attention function with Softmax never allocates exactly zero weight to any node, thereby allowing each node access to the entire graph. Concurrently, to capture information from closely related nodes, a sparse branch denoted as f_s with Top- k sparse attention layers is introduced. Both branches adaptively fuse information at the end of each layer.

Finally, the output from the global branch, $H_g^{(L)}$, is used for autoregressive decoding, with the likelihood of node selection being primarily determined by the similarity of the nodes' embeddings.

a) *Global Layer*: Each layer involves a MHA [67] and a SwiGLU [72], along with RMSNorm [42] and residual connections [73]. The i -th layer is formulated as follows:

$$\hat{H}_g^{(i)} = \text{RMSNorm}^{(i)} \left(H_g^{(i-1)} + \text{MHA}^{(i)} \left(H_g^{(i-1)}, \text{Concat}[H_g^{(i-1)}, P^{(i-1)}] \right) \right), \quad (9)$$

$$\tilde{H}_g^{(i)} = \text{RMSNorm}^{(i)} \left(\hat{H}_g^{(i)} + \text{SwiGLU}^{(i)}(\hat{H}_g^{(i)}) \right), \quad (10)$$

$$\hat{P}^{(i)} = \text{RMSNorm}^{(i)} \left(P^{(i-1)} + \text{MHA}^{(i)} \left(P^{(i-1)}, \text{Concat}[H_g^{(i-1)}, P^{(i-1)}] \right) \right), \quad (11)$$

$$P^{(i)} = \text{RMSNorm}^{(i)} \left(\hat{P}^{(i)} + \text{SwiGLU}^{(i)}(\hat{P}^{(i)}) \right), \quad (12)$$

where $H_g^{(i-1)} \in \mathbb{R}^{(N+1) \times d_h}$ represents the node embeddings output from the $(i-1)$ -th global layer.

b) *Sparse Layer*: In the sparse branch f_s , each layer also consists of an attention layer and a SwiGLU activation function. However, to focus more precisely on related nodes, we replace the attention function $\text{Attention}(\cdot, \cdot)$ in $\text{MHA}(\cdot, \cdot)$ with $\text{SparseAtt}(\cdot, \cdot)$, which masks attention scores smaller

than the Top- k scores by setting them to zero. This can be formulated as follows:

$$\text{SparseAtt}(X, Y) = \text{Softmax}(M(\mathbf{A}))YW_V, \quad (13)$$

where \mathbf{A} is the attention scores calculated as shown in Equation 5. $M(\cdot)$ is the Top- k selection operation:

$$[M(\mathbf{A})]_{ij} = \begin{cases} \mathbf{A}_{ij} & \text{if } \mathbf{A}_{ij} \in \text{Top-}k(\mathbf{A}_{i*}), \\ 0 & \text{otherwise.} \end{cases} \quad (14)$$

where \mathbf{A}_{i*} represents the attention scores of the i -th node with all other nodes, i.e., $\mathbf{A}_{i*} = \{\mathbf{A}_{ij} \mid j \in \{0, 1, \dots, N\}\}$, and the Top- k operation selects the top k highest attention scores from this set.

c) Fusion Layer: In our model, a simple linear projection is applied at the end of each layer to transform embeddings between two branches. For the i -th layer, the outputs from the global and sparse branches are denoted as $\tilde{H}_g^{(i)}$ and $\tilde{H}_s^{(i)}$, respectively. The final outputs are given by:

$$H_g^{(i)} = \tilde{H}_g^{(i)} + (\tilde{H}_s^{(i)}W_s + b_s), \quad (15)$$

$$H_s^{(i)} = \tilde{H}_s^{(i)} + (\tilde{H}_g^{(i)}W_g + b_g), \quad (16)$$

where W_s , b_s , W_g , and b_g are learnable parameters.

D. Decoder

After encoding, the output of the global branch, $H^{(L)} = [\mathbf{h}_0^{(L)}, \mathbf{h}_1^{(L)}, \dots, \mathbf{h}_N^{(L)}]$, is utilized to construct the solution. During the autoregressive decoding process, at step t , the context embedding is defined as:

$$H_c = \text{Concat}[\mathbf{h}_{\tau_t}^{(L)}, c_t^l, c_t^b, z_t, l_t, o_t]W_t, \quad (17)$$

where τ_t is the partial solution already generated, and τ_t is the last node of the partial solution. The terms c_t^l, c_t^b represent the remaining capacity of the vehicle for linehaul and backhaul customers, respectively. The terms z_t, l_t , and o_t represent the current time, the remaining length of the current partial route (if the problem includes a length limitation), and the presence indicator of the open route, respectively. The matrix $W_c \in \mathbb{R}^{(d_h+5) \times d_h}$ is a learnable parameter.

Then the context embeddings are processed through a MHA to generate the final query:

$$q_c = \text{MHA}(H_c^{(L)}, \text{Concat}[\mathbf{h}_i^{(L)} : i \in I_t]), \quad (18)$$

where I_t represents the set of feasible actions at the current step. The compatibility u_i is computed as:

$$u_i = \begin{cases} \xi \cdot \tanh\left(\frac{q_c(\mathbf{h}_i^{(L)})^\top}{\sqrt{d_k}}\right) & \text{if } i \in I_t, \\ -\infty & \text{otherwise,} \end{cases} \quad (19)$$

where ξ is a predefined clipping hyperparameter. Finally, the action probabilities $\pi_\theta(\tau_g = i \mid \mathcal{V}, \tau_{1:g-1})$ are obtained by applying the Softmax function to $u = \{u_i\}_{i \in I}$.

Additionally, to determine the set of feasible actions at the current step I_t , we utilize the following feasibility testing process.

- 1) Each customer node can only be visited once. If the depot is the last action in a partial solution, the next action cannot be the depot (to avoid a self-loop).

$$i \in \tau_{1:t-1}, i \in \{1, 2, \dots, N\} \Rightarrow i \notin I_t, \quad (20)$$

$$\tau_{t-1} = 0 \Rightarrow 0 \notin I_t. \quad (21)$$

- 2) For a problem without the Open Route constraint ($V_1 = 0$), each sub-route needs to return to the depot v_0 within the given limit. There are two types of constraints that enforce limits on when each sub-route must reach the depot: the Time Window constraint ($V_2 = 1$) with a time limit \mathcal{T} , and the Distance Limit constraint ($V_3 = 1$) with a distance limit ρ .

$$\begin{aligned} & (V_1 = 0) \wedge (V_2 = 1) \wedge ((z_t + d_{\tau_{t-1}i} + s_i + d_{i0}) > \mathcal{T}) \\ & \vee ((V_1 = 0) \wedge (V_3 = 1) \wedge (l_t < d_{\tau_{t-1}i} + d_{i0})) \\ & \Rightarrow i \notin I_t. \end{aligned} \quad (22)$$

- 3) For problems with a Time Window constraint ($V_2 = 1$), each customer node v_i has a time window $[e_i, l_i]$ and a service time s_i . The vehicle must visit v_i and complete its service within the specified time window.

$$(V_2 = 1) \wedge (z_t + d_{\tau_{t-1}i} + s_i > l_i) \Rightarrow i \notin I_t. \quad (23)$$

- 4) For the problem with the Backhaul constraint ($V_4 = 1$), the backhaul will be masked if there are still linehaul services that have not been completed.

$$\begin{aligned} & (\delta_i < 0) \wedge (\exists j \in \{1, 2, \dots, N\}(\delta_j > 0) \wedge (j \notin \tau_{1:t-1})) \\ & \Rightarrow i \notin I_t. \end{aligned} \quad (24)$$

- 5) For customers, service is available when their demand does not exceed the current available capacity.

$$\begin{aligned} & ((\delta_i > 0) \wedge (\delta_i > c_t^l)) \vee ((\delta_i < 0) \wedge (-\delta_i > c_t^b)) \\ & \Rightarrow i \notin I_t. \end{aligned} \quad (25)$$

V. EXPERIMENTS

To evaluate the effectiveness of the proposed CaDA for VRPs, we conduct experiments on 16 different VRP variants with five constraints. Furthermore, we perform ablation studies to validate the efficiency of the proposed components.

A. Problem Setup

In this section, we provide a detailed description of the VRP problems setup used in this study.

a) Locations: The nodes' locations are represented by a two-dimensional vector $\vec{X}_i, i \in \{0, \dots, N\}$, and are derived from a uniform distribution $U(0, 1)$.

b) Capacity: In this study, we consider only homogeneous vehicles, with the same vehicle capacity C shared among all vehicles, and the number of vehicles is unlimited. Following the common capacity setup used in previous studies [4], [6], for $N = 50$ and $N = 100$, the vehicle capacity C is set to 40 and 50 respectively.

c) *Node Demands*: In our study, there are two types of customers: linehaul customers with demand $\delta_i < 0$ and backhaul customers with $\delta_i > 0$ (when the backhaul constraint is active). We generate node demands as follows: we generate linehaul demands δ_i^l for all customers $i \in \{1, \dots, N\}$ by uniform sampling from the set of integers $\{1, 2, \dots, 9\}$. If the backhaul constraint is inactive, each node’s true demands δ_i are equal to δ_i^l . The demand generation process is now complete. Otherwise, we generate backhaul demands δ_i^b by sampling uniformly from the same set of integers $\{1, 2, \dots, 9\}$. Subsequently, generate a temporary variable $y_i \sim U(0, 1)$ for each customer i . The demand δ_i for each customer i is determined by the following rule:

$$\delta_i = \begin{cases} \delta_i^l & \text{if } y_i \geq 0.2, \\ \delta_i^b & \text{otherwise.} \end{cases} \quad (26)$$

For each node, there is a 20% probability that it represents backhaul customers in an instance.

Furthermore, before passing the demands δ_i to the policy, for training stability, we normalize the demand δ_i to the range $[0, 1]$ by $\delta_i' = \frac{\delta_i}{C}$. We set the normalized capacity to 1 to ensure that at each step of the decoding process, the remaining capacity c_t also falls within the range $[0, 1]$.

d) *Time Windows*: For problems with time window constraints, several related factors must be considered: time windows $[e_i, l_i]$ and service times s_i . For the depot, $e_0 = s_0 = 0$, $l_0 = \mathcal{T} = 4.6$, where \mathcal{T} represents the overall time limit for each sub-route. Additionally, the vehicle speed is 1.0.

For customers $i \in \{1, 2, \dots, N\}$, service times s_i are uniformly sampled from $[0.15, 0.18]$. Additionally, time window lengths Δt_i are uniformly sampled from $[0.18, 0.2]$. Moreover, each customer’s time window must be feasible for the tour $(0, i, 0)$; otherwise, there is no feasible tour to service this customer. Consequently, the upper bounds for the start times of the time windows are calculated as:

$$e_i^{\text{up}} = \frac{\mathcal{T} - s_i - \Delta t_i}{d_{0i}} - 1. \quad (27)$$

Subsequently, the start times of the time windows e_i are determined as follows:

$$e_i = (1 + (e_i^{\text{up}} - 1) \cdot y_i) \cdot d_{0i}, \quad (28)$$

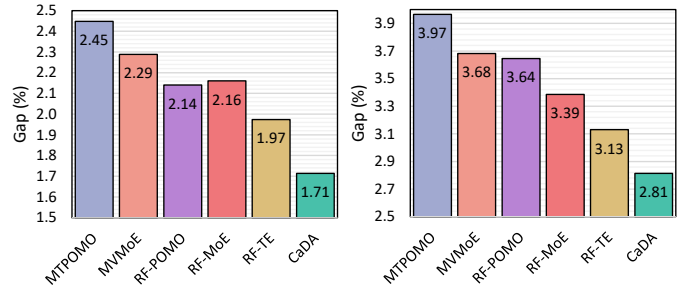
where $y_i \sim U(0, 1)$. Finally, the end times of the time windows are determined by:

$$l_i = e_i + \Delta t_i. \quad (29)$$

e) *Distance Limit*: For problems with the Distance Limit constraint, each sub-tour must be completed within a limit ρ . To ensure each instance has a feasible solution, i.e., the length of the tour $(0, i, 0)$ should remain within this limit, ρ is sampled from $U(2 \cdot \max(d_{0*}), \rho_{\max})$, where $\rho_{\max} = 3.0$ is a predefined upper bound.

TABLE II
EXPERIMENT HYPERPARAMETERS.

Hyperparameter	Value
Model	
Embedding dimension d_h	128
Number of attention heads M_h	8
Number of encoder layers L	6
Top- k	$\frac{(N)}{2}$
Feedforward hidden dimension d_a	512
Tanh clipping ξ	10.0
Training	
Batch size	256
Train data per epoch	100,000
Optimizer	AdamW [74]
Learning rate (LR)	$3e^{-4}$
Weight decay	$1e^{-6}$
LR scheduler	MultiStepLR
LR milestones	[270, 295]
LR gamma	0.1
Gradient clip value	1.0
Training epochs	300
Number of tasks used for training	16



(a) Average gap of different neural solvers on VRPs with 50 nodes. (b) Average gap of different neural solvers on VRPs with 100 nodes.

Fig. 3. Comparison results of CaDA with state-of-the-art cross-problem neural solvers, showing the average gap on 16 VRPs.

B. Baselines

We utilize state-of-the-art traditional and neural solvers as baselines. For the traditional approaches, we employ two open-source solvers capable of addressing all 16 VRPs in this study: PyVRP [75], which extends the state-of-the-art heuristic algorithm HGS-CVRP [76], and Google’s OR-Tools. Both baseline methods solve each instance using a single CPU core, with a time limit of 10 seconds for VRP50 and 20 seconds for VRP100, respectively. For the neural solvers, we compare our method against representative multi-task learning models: MTPOMO [15], MVMoE [16], and RouteFinder [17], including RF-POMO, RF-MoE, and RF-TE. We utilize the open-source code published by RouteFinder [17]. For each method, we separately train two models from scratch on VRP50 and VRP100 using the same hyperparameter settings in RouteFinder [17]. However, for RF-MoE and MVMoE, due to their higher memory demands, we utilize the pre-trained

TABLE III
PERFORMANCE ON 1000 TEST INSTANCES OF 16 VRPs. THE BEST LEARNING-BASED RESULTS FOR EACH DATASET ARE HIGHLIGHTED WITH A GRAY BACKGROUND.

	Solver	n = 50			n = 100			Solver	n = 50			n = 100		
		Obj.	Gap	Time	Obj.	Gap	Time		Obj.	Gap	Time	Obj.	Gap	Time
CVRP	HGS-PyVRP	10.372	*	10.4m	15.628	*	20.8m	HGS-PyVRP	16.031	*	10.4m	25.423	*	20.8m
	OR-Tools	10.572	1.907%	10.4m	16.280	4.178%	20.8m	OR-Tools	16.089	0.347%	10.4m	25.814	1.506%	20.8m
	MTPOMO	10.520	1.423%	2s	15.941	2.030%	8s	MTPOMO	16.419	2.423%	2s	26.433	3.962%	9s
	MVMoE	10.499	1.229%	3s	15.888	1.693%	11s	MVMoE	16.400	2.298%	3s	26.390	3.789%	11s
	RF-POMO	10.506	1.300%	2s	15.908	1.833%	8s	RF-POMO	16.363	2.066%	2s	26.361	3.675%	9s
	RF-MoE	10.499	1.225%	3s	15.877	1.625%	11s	RF-MoE	16.389	2.232%	3s	26.321	3.516%	11s
	RF-TE	10.502	1.257%	2s	15.860	1.524%	8s	RF-TE	16.341	1.933%	2s	26.228	3.154%	8s
	CaDA	10.494	1.182%	2s	15.870	1.578%	8s	CaDA	16.278	1.536%	2s	26.070	2.530%	8s
OVRP	HGS-PyVRP	6.507	*	10.4m	9.725	*	20.8m	HGS-PyVRP	10.587	*	10.4m	15.766	*	20.8m
	OR-Tools	6.553	0.686%	10.4m	9.995	2.732%	20.8m	OR-Tools	10.570	2.343%	10.4m	16.466	5.302%	20.8m
	MTPOMO	6.717	3.194%	2s	10.216	5.028%	8s	MTPOMO	10.775	1.733%	2s	16.157	2.483%	8s
	MVMoE	6.705	3.003%	3s	10.177	4.617%	11s	MVMoE	10.753	1.525%	3s	16.099	2.113%	11s
	RF-POMO	6.699	2.926%	2s	10.190	4.761%	8s	RF-POMO	10.748	1.498%	2s	16.117	2.241%	8s
	RF-MoE	6.697	2.880%	3s	10.139	4.234%	11s	RF-MoE	10.737	1.390%	3s	16.070	1.937%	11s
	RF-TE	6.682	2.658%	2s	10.115	3.996%	8s	RF-TE	10.747	1.485%	2s	16.057	1.858%	8s
	CaDA	6.670	2.468%	2s	10.121	4.045%	8s	CaDA	10.731	1.333%	2s	16.057	1.847%	8s
VRPB	HGS-PyVRP	9.687	*	10.4m	14.377	*	20.8m	HGS-PyVRP	10.510	*	10.4m	16.926	*	20.8m
	OR-Tools	9.802	1.159%	10.4m	14.933	3.853%	20.8m	OR-Tools	10.519	0.078%	10.4m	17.027	0.583%	20.8m
	MTPOMO	10.036	3.596%	2s	15.102	5.052%	8s	MTPOMO	10.676	1.558%	2s	17.442	3.022%	9s
	MVMoE	10.007	3.292%	3s	15.023	4.505%	10s	MVMoE	10.674	1.541%	3s	17.416	2.870%	12s
	RF-POMO	9.992	3.135%	2s	15.025	4.534%	8s	RF-POMO	10.656	1.361%	2s	17.405	2.809%	9s
	RF-MoE	9.980	3.017%	3s	14.973	4.168%	10s	RF-MoE	10.674	1.540%	3s	17.388	2.704%	12s
	RF-TE	9.979	3.000%	2s	14.935	3.906%	8s	RF-TE	10.645	1.264%	2s	17.328	2.352%	9s
	CaDA	9.960	2.800%	2s	14.960	4.038%	8s	CaDA	10.613	0.957%	2s	17.226	1.751%	9s
VRPBL	HGS-PyVRP	10.186	*	10.4m	14.779	*	20.8m	HGS-PyVRP	18.361	*	10.4m	29.026	*	20.8m
	OR-Tools	10.331	1.390%	10.4m	15.426	4.338%	20.8m	OR-Tools	18.422	0.332%	10.4m	29.830	2.770%	20.8m
	MTPOMO	10.679	4.760%	2s	15.718	6.294%	8s	MTPOMO	19.001	2.199%	3s	30.948	3.794%	9s
	MVMoE	10.639	4.384%	3s	15.642	5.771%	11s	MVMoE	18.983	2.097%	3s	30.892	3.609%	12s
	RF-POMO	10.590	3.926%	2s	15.632	5.725%	8s	RF-POMO	18.938	1.863%	2s	30.847	3.452%	9s
	RF-MoE	10.575	3.765%	3s	15.542	5.125%	10s	RF-MoE	18.957	1.960%	3s	30.809	3.325%	12s
	RF-TE	10.569	3.713%	2s	15.523	5.008%	8s	RF-TE	18.910	1.713%	2s	30.705	2.978%	9s
	CaDA	10.543	3.461%	2s	15.525	5.001%	8s	CaDA	18.848	1.376%	2s	30.520	2.359%	9s
VRPBLTW	HGS-PyVRP	18.292	*	10.4m	29.467	*	20.8m	HGS-PyVRP	16.356	*	10.4m	25.757	*	20.8m
	OR-Tools	18.366	0.383%	10.4m	29.945	1.597%	20.8m	OR-Tools	16.441	0.499%	10.4m	26.259	1.899%	20.8m
	MTPOMO	18.649	1.938%	2s	30.478	3.426%	9s	MTPOMO	16.832	2.877%	2s	26.913	4.455%	9s
	MVMoE	18.632	1.841%	3s	30.437	3.284%	12s	MVMoE	16.817	2.783%	3s	26.866	4.272%	12s
	RF-POMO	18.603	1.684%	2s	30.384	3.102%	9s	RF-POMO	16.756	2.419%	2s	26.818	4.084%	9s
	RF-MoE	18.616	1.757%	3s	30.340	2.951%	12s	RF-MoE	16.777	2.548%	3s	26.773	3.910%	12s
	RF-TE	18.573	1.517%	2s	30.249	2.641%	9s	RF-TE	16.728	2.248%	2s	26.706	3.645%	9s
	CaDA	18.500	1.117%	2s	30.059	1.999%	9s	CaDA	16.669	1.879%	2s	26.540	2.995%	9s
OVRPB	HGS-PyVRP	6.898	*	10.4m	10.335	*	20.8m	HGS-PyVRP	6.899	*	10.4m	10.335	*	20.8m
	OR-Tools	6.928	0.412%	10.4m	10.577	2.315%	20.8m	OR-Tools	6.927	0.386%	10.4m	10.582	2.363%	20.8m
	MTPOMO	7.105	2.973%	2s	10.882	5.264%	8s	MTPOMO	7.112	3.053%	2s	10.888	5.318%	8s
	MVMoE	7.089	2.744%	3s	10.841	4.869%	11s	MVMoE	7.094	2.799%	3s	10.847	4.929%	11s
	RF-POMO	7.085	2.686%	2s	10.839	4.857%	8s	RF-POMO	7.088	2.703%	2s	10.842	4.883%	8s
	RF-MoE	7.081	2.617%	3s	10.806	4.528%	11s	RF-MoE	7.082	2.630%	3s	10.807	4.537%	11s
	RF-TE	7.065	2.385%	2s	10.774	4.233%	8s	RF-TE	7.068	2.417%	2s	10.778	4.266%	8s
	CaDA	7.049	2.159%	2s	10.762	4.099%	8s	CaDA	7.051	2.166%	2s	10.762	4.102%	8s
OVRPBLTW	HGS-PyVRP	11.668	*	10.4m	19.156	*	20.8m	HGS-PyVRP	11.669	*	10.4m	19.156	*	20.8m
	OR-Tools	11.681	0.106%	10.4m	19.305	0.767%	20.8m	OR-Tools	11.682	0.109%	10.4m	19.303	0.757%	20.8m
	MTPOMO	11.823	1.315%	3s	19.658	2.602%	9s	MTPOMO	11.823	1.307%	3s	19.656	2.592%	9s
	MVMoE	11.816	1.249%	4s	19.640	2.514%	12s	MVMoE	11.816	1.245%	4s	19.637	2.499%	13s
	RF-POMO	11.810	1.192%	3s	19.618	2.393%	10s	RF-POMO	11.809	1.182%	3s	19.620	2.403%	10s
	RF-MoE	11.824	1.309%	4s	19.607	2.334%	12s	RF-MoE	11.823	1.303%	4s	19.605	2.324%	12s
	RF-TE	11.789	1.017%	2s	19.554	2.061%	9s	RF-TE	11.790	1.027%	2s	19.555	2.062%	9s
	CaDA	11.760	0.771%	2s	19.435	1.439%	9s	CaDA	11.761	0.779%	2s	19.436	1.441%	9s
OVRPL	HGS-PyVRP	6.507	*	10.4m	9.724	*	20.8m	HGS-PyVRP	10.510	*	10.4m	16.926	*	20.8m
	OR-Tools	6.552	0.668%	10.4m	10.001	2.791%	20.8m	OR-Tools	10.497	0.114%	10.4m	17.023	0.728%	20.8m
	MTPOMO	6.720	3.248%	2s	10.224	5.112%	8s	MTPOMO	10.677	1.572%	2s	17.442	3.020%	9s
	MVMoE	6.706	3.028%	3s	10.184	4.693%	11s	MVMoE	10.677	1.564%	3s	17.418	2.880%	12s
	RF-POMO	6.701	2.944%	2s	10.190	4.762%	8s	RF-POMO	10.656	1.362%	3s	17.404	2.802%	9s
	RF-MoE	6.695	2.859%	3s	10.140	4.252%	11s	RF-MoE	10.673	1.531%	3s	17.386	2.696%	12s
	RF-TE	6.683	2.680%	2s	10.121	4.054%	8s	RF-TE	10.646	1.267%	2s	17.328	2.352%	9s
	CaDA	6.671	2.475%	2s	10.122	4.052%	8s	CaDA	10.613	0.961%	2s	17.226	1.752%	9s

TABLE IV
AVERAGE OBJECTIVE FUNCTION VALUE AND GAP ACROSS 16 VRPs FOR ABLATION MODELS AND CaDA.

	Obj.	Gap
CaDA w/o Prompt	11.534	1.926%
CaDA w/o Sparse	11.521	1.795%
CaDA	11.513	1.714%

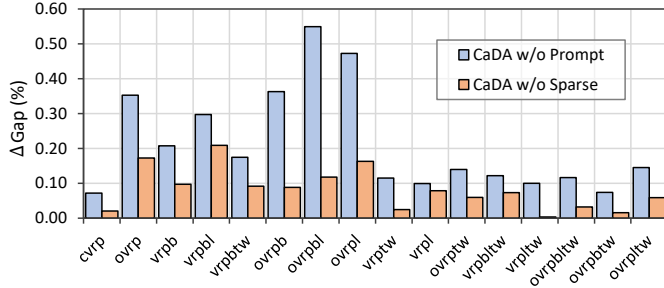


Fig. 4. Ablation study on the proposed components of CaDA across 16 VRPs. The height of the bars represents the increased gap in performance between the model with specific components ablated and the baseline CaDA.

parameters provided by RouteFinder [17] and test them under the same hardware settings as ours. For our method CaDA, we also train two models on VRP50 and VRP100, with the hyperparameters summarized in Table II. All neural methods utilize the same training data budget.

C. Testing and Hardware

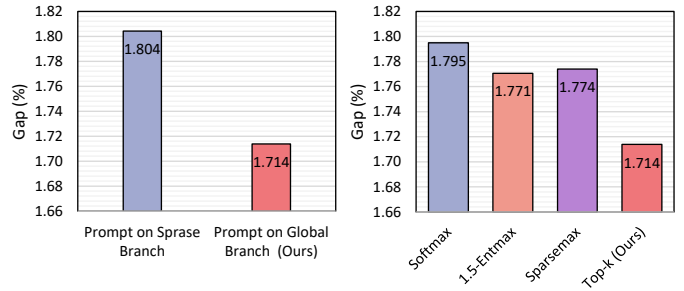
We utilize the test dataset published by Routefinder [17], which includes 1K randomly generated instances for each VRP variant, at scales of 50 and 100. All neural solvers are tested on the same scale as their training scale. For all neural solvers, we employ a greedy rollout strategy with $\times 8\text{aug}$ [4]. This approach conducts equivalent transformations to augment the original instance and reports the best results among the eight augmented instances.

All computational experiments are conducted on a platform equipped with NVIDIA GeForce RTX 3090 GPUs and Intel(R) Xeon(R) Gold 6348 CPUs at 2.60 GHz. Under these conditions, training our model from scratch for VRP50 takes approximately 17 hours, and about 25 hours for VRP100.

D. Main Results

In Table III, we report the average performances for each dataset and the gaps compared to the best-performing traditional VRP solvers, as indicated by asterisks (*). Additionally, we present the total time required to solve the dataset. The best learning-based results for each dataset are highlighted with a gray background. Furthermore, we present the comparison results with the average gap on 16 VRPs for both 50-node and 100-node instances in Figure 3.

Results illustrate that the proposed CaDA method can effectively manage various VRP variants at different scales. Specifically, for VRP50 and VRP100, CaDA surpasses the



(a) CaDA with different prompt positions: concatenated to the input of the sparse branch, and with-sparse branch, and concatenated to the out sparse operations (i.e., using only input of the global branch, where the standard softmax in both branches), latter is the standard setting. (b) CaDA with different sparse operations: concatenated to the input of the sparse branch, and with-sparse branch, and concatenated to the out sparse operations (i.e., using only input of the global branch, where the standard softmax in both branches), latter is the standard setting. where Top- k is the standard setting.

Fig. 5. The average gap across 16 VRPs for CaDA variants under different model settings.

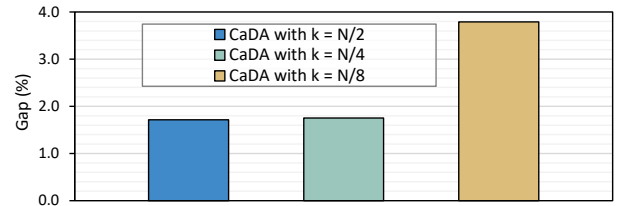


Fig. 6. Average gap on 16 VRPs for CaDA variants with different k values in the Top- k selection operation, where $k = \frac{N}{2}$ is the standard setting.

second-best method by 0.26% and 0.32%, respectively. It ranks first among all neural network-based solvers for all VRP50 variants and for 13 out of 16 VRP100 variants. Similar to other neural solvers, CaDA significantly reduces the running time compared to state-of-the-art heuristic solvers.

E. Ablation Study

In this section, we conduct ablation studies to validate the efficacy of the proposed components in CaDA. Specifically, we separately remove the constraint prompt and the Top- k operation, resulting in two CaDA variants: CaDA w/o prompt and CaDA w/o Sparse, where 'w/o' stands for 'without.' In CaDA w/o Sparse, both branches use the standard Softmax with global connectivity. CaDA and its variants are trained and evaluated on VRP50. During testing, $\times 8\text{aug}$ [4] is employed.

The results in Table IV show the average gap on 16 VRPs and demonstrate that all components of CaDA make substantial contributions, with the prompt playing a particularly important role. Additionally, to study the effect of different components on various problems, we demonstrate the increased gap of these two ablation models compared with CaDA on different VRP datasets in Figure 4. These results illustrate that both the prompt and the sparse operation improve performance on all VRP variants.

Then, we further explore the influence of different CaDA settings. Specifically, using CaDA as the baseline, we conduct experiments on VRP50 focusing on the following aspects:

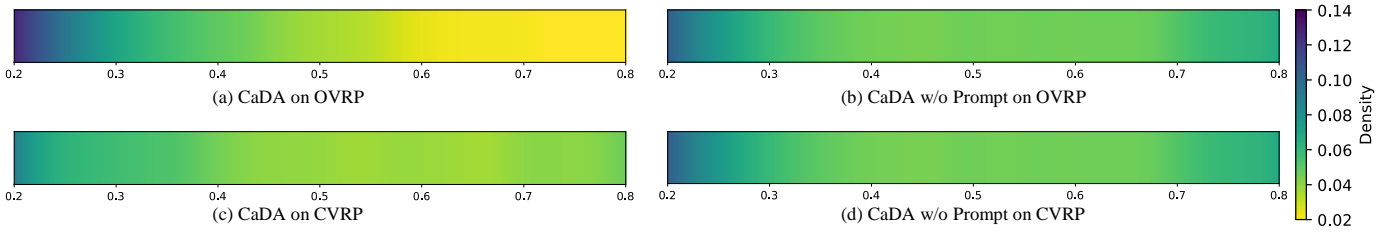


Fig. 7. The distribution of attention weights between customers and the depot $\mathbf{A}_{i0}, i \in \{1, 2, \dots, N\}$ for CaDA and CaDA w/o Prompt on CVRP and OVRP. Kernel Density Estimation (KDE) with Gaussian kernels is applied to estimate the attention weight distribution, which is visualized using a heatmap. CaDA w/o Prompt exhibits a similar attention distribution across both problems, leading to increased interference between tasks. In contrast, CaDA shows a significantly lower density of high attention values for OVRP, indicating that the proposed prompt effectively provides constraint information as depot will never be the next action for any customer in OVRP.

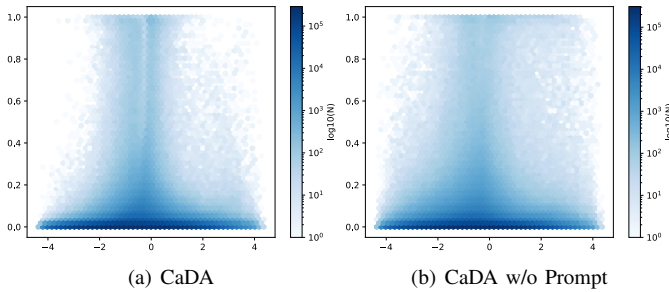


Fig. 8. For 100 VRPTW instances, the distribution of attention scores \mathbf{A}_{ij} across varying $\mathbf{P}_{i,j}$, where \mathbf{A}_{ij} is the attention score from node v_i to node v_j , and $\mathbf{P}_{i,j} = (l_j - e_i) - d_{ij} - (s_i + s_j)$ represents the surplus time when the vehicle starts from v_i at time e_i and travels to v_j . If $\mathbf{P}_{i,j} < 0$, the edge (i, j) is illegal; if $\mathbf{P}_{i,j}$ becomes too large, including (i, j) in the solution may result in the vehicle having to wait a long time for v_j to open. The shade represents the density in that region. For CaDA, the attention scores at extremely high and low $\mathbf{P}_{i,j}$ values are diminished, indicating that the model successfully comprehends the time window constraint.

a) *Position of Prompt*: We consider two positions to introduce prompts: the input for the global branch (i.e., CaDA), and the input for the sparse branch. Figure 5(a) illustrates the average gap across 16 VRPs of the different models. The results indicate that integrating both sparse and prompt mechanisms within the same branch yields inferior performance compared to placing the prompt in the global branch. This is because the prompt in the sparse branch may be masked by the sparse function, leading to insufficient constraint information, which diminishes model performance.

b) *Different Sparse Function*: To validate the efficacy of our Top- k sparse operation, we replace the Softmax+Top- k in our CaDA with a standard Softmax and a representative sparse function α -entmax with two configurations: $\alpha = 1.5$, referred to as 1.5-entmax [64], and $\alpha = 2$, which corresponds to sparsemax [63].

Figure 5(b) shows the average gap across 16 VRPs. Firstly, three versions of CaDA that incorporate different sparse functions consistently outperform the version of CaDA with standard Softmax, which only has global connectivity. This indicates that the model benefits from focusing on promising nodes. Furthermore, the Top- k operation outperforms the other two sparse operations, demonstrating its effectiveness for

TABLE V
AVERAGE OBJECTIVE FUNCTION VALUE AND GAP ACROSS 16 VRPs FOR ABLATION MODELS AND CaDA.

k	Obj.	Gap
10	6440.8	4.61%
25	6431.8	4.17%
50	6458.6	4.79%
75	6463.7	4.88%
100	6475.7	5.15%

VRPs.

c) *k for Top- k* : To explore the different k values' effects on CaDA, we conducted experiments with $k \in \{\frac{N}{2}, \frac{N}{4}, \frac{N}{8}\}$ and trained these models from scratch respectively. Figure 6 shows the average gap on 16 VRP50 datasets. While $k = \frac{N}{2}$ demonstrates the best performance, $k = \frac{N}{4}$ performs slightly worse, and the performance of $k = \frac{N}{8}$ drops dramatically. It indicates that when $k = \frac{N}{2}$, the sparse branch can better cooperate with the global branch. This is the standard setting for CaDA.

F. Visualization of Constraint Awareness

To explore the influence of the prompt, we conducted further statistical experiments on the distribution of attention scores within the encoder. All experiments mentioned below involve 100 VRP50 instances randomly selected from the test dataset, and attention scores were collected from all heads across all global layers.

a) *Influence on Open Route Constraint*: In the case of the Open Route constraint, where the vehicle does not return to the depot v_0 , the depot will never be the next node for any customer node v_i . Whereas in CVRP, the vehicle must return to the depot, making it a potential next node for any customer. As a result, the model should exhibit different customer-depot attention patterns for CVRP and OVRP. Specifically, in CVRP, the model should exhibit a greater number of high attention scores \mathbf{A}_{i0} compared to OVRP.

Figure 7 shows the distribution of \mathbf{A}_{i0} for CaDA and CaDA w/o Prompt on CVRP and OVRP. We apply Kernel Density Estimation (KDE) with Gaussian kernels to estimate the distribution of attention weights between 0.2 and 0.8.

TABLE VI
RESULTS ON CVRPLIB DATASETS.

Opt.	MTPOMO		MVMoE		RF-POMO		RF-MoE		RF-TE		CaDA ₂₅		CaDA ₂₅ × 32		
	Obj.	Gap	Obj.	Gap	Obj.	Gap	Obj.	Gap	Obj.	Gap	Obj.	Gap	Obj.	Gap	
Set A	1041.9	1087.9	5.07%	1071.3	3.07%	1064.1	2.11%	1072.2	2.83%	1070.3	2.86%	1069.9	2.76%	1062.9	2.00%
Set B	963.7	1006.9	4.86%	999.2	3.94%	991.6	2.89%	994.0	3.17%	987.4	2.58%	987.5	2.58%	982.7	2.02%
Set F	707.7	820.0	16.23%	770.5	7.38%	804.0	13.93%	813.0	14.31%	794.7	12.95%	748.7	5.74%	745.3	4.99%
Set P	587.4	629.3	11.10%	1144.0	5.31%	606.4	4.72%	603.3	3.39%	608.7	4.59%	607.9	4.82%	601.2	3.16%
Set X	27220.1	28952.5	6.09%	614.0	6.76%	28825.4	5.54%	29125.2	6.37%	28520.3	4.46%	28745.0	4.97%	28573.9	4.41%
Avg.	6104.2	6499.3	8.67%	919.8	5.29%	6458.3	5.84%	6521.5	6.01%	6396.3	5.49%	6431.8	4.17%	6393.2	3.32%

The bandwidth parameter is set to 0.1, and the KDE is visualized using a heatmap. Firstly, CaDA exhibits a significantly different distribution of attention scores between CVRP and OVRP, whereas CaDA w/o Prompt shows a similar attention distribution across both problems, which increases the interference between different tasks. Furthermore, when comparing CaDA on CVRP and CaDA on OVRP, we observe a significantly lower density of high attention values for OVRP, indicating that the proposed prompt effectively provides constraint information and helps the model better understand the problem.

b) Influence on Time Window Constraint: For the Time Window constraint, nodes v_i can only be visited within their respective time windows (e_i, l_i) , and serving each customer costs s_i time. Thus, the relationship between node pairs (v_i, v_j) is influenced by their time-related factors and positional distances, i.e., (e_i, l_i, s_i) , (e_j, l_j, s_j) , and d_{ij} .

If an edge (i, j) is legal, then it must satisfy $e_i + s_i + d_{ij} \leq l_j - s_j$. This condition means that if a vehicle starts at time e_i , spends s_i time servicing v_i , and takes d_{ij} time to reach v_j , it must arrive by $(l_j - s_j)$ at the latest to successfully service v_j and leave the node within the service window. Accordingly, we derive the following inequality:

$$\begin{aligned} e_i + s_i + d_{ij} &\leq l_j - s_j \\ \implies (l_j - e_i) - d_{ij} - (s_i + s_j) &\geq 0 \end{aligned} \quad (30)$$

Define $\mathbf{P}_{i,j} = (l_j - e_i) - d_{ij} - (s_i + s_j)$. Figure 8 visualizes the distribution of \mathbf{A}_{ij} across varying $\mathbf{P}_{i,j}$. Firstly, CaDA exhibits fewer high attention values for $\mathbf{P}_{i,j} < 0$. Additionally, for $\mathbf{P}_{i,j}$ values that are too high, the vehicle may need to wait a long time at v_j to wait until the start of the time window e_j . For example, consider $\mathbf{P}_{i,j} = 4$ while the overall time limit for the sub-route is $\mathcal{T} = 4.6$. Including the edge (i, j) in the solution may result in significant time wasted waiting. Compared to the CaDA w/o Prompt, CaDA also exhibits fewer high attention values for $\mathbf{P}_{i,j} > 3$, indicating that CaDA more efficiently understands the problem constraints.

G. Result on Real-World Instances

To further validate the effectiveness of CaDA in real-world instances, we conducted experiments using five test suites from CVRPLib¹ benchmark datasets. These datasets comprise

¹<http://vrp.atd-lab.inf.puc-rio.br/>

a total of 101 instances from Sets A, B, F, P, and X [77], with graph scales ranging from 16 to 200, various node distributions, and customer demands. CaDA is trained on 16 different VRP types, each with a graph size of 100 nodes.

We initially explore the effect of different k values on the Top- k sparse operation during testing. Table V demonstrates the average gap compared to the best-known results from CVRPLIB across all instances when testing CaDA with different $k \in \{10, 25, 50, 100\}$. The results show that when $k = 25$, CaDA achieves the best performance across different scales.

Furthermore, we compared CaDA with existing cross-problem neural solvers. We additionally provide a $\times 32$ data augmentation method for CaDA, which reports the best solution among utilizing 32 prompts. Specifically, we generate all possible combinations of 5-dimensional binary vector V (i.e., 2^5), which is simple to implement and efficient to execute in batches. Table VI exhibits the comparison results of five test suites with the average objective function values, the gap with the best-known solution for each dataset. The best results for each dataset are highlighted in bold. CaDA₂₅ represents CaDA tested with $k = 25$. Results demonstrate that the proposed CaDA₂₅ × 32 achieves the best performance among the learning methods.

VI. CONCLUSION

In this paper, we have proposed the Constraint-Aware Dual-Attention Model (CaDA), a novel cross-problem neural solver for VRPs. CaDA incorporates a constraint prompt and a dual-attention mechanism, which consists of a global branch and a sparse branch, to efficiently generate constraint-aware node embeddings. We have thoroughly evaluated CaDA across 16 VRP variants and real-world benchmark instances. CaDA shows superior performance when compared to current leading neural solvers. Additional ablation studies confirm the effectiveness of the proposed constraint prompt and the dual-attention model structure.

REFERENCES

- [1] D. Cattaruzza, N. Absi, D. Feillet, and J. González-Feliu, “Vehicle routing problems for city logistics,” *EURO Journal on Transportation and Logistics*, vol. 6, no. 1, pp. 51–79, 2017.
- [2] J.-P. Rodrigue, *The geography of transport systems*, 5th ed. New York: Routledge, 2020.
- [3] Y. Bengio, A. Lodi, and A. Prouvost, “Machine learning for combinatorial optimization: a methodological tour d’horizon,” *European Journal of Operational Research*, vol. 290, no. 2, pp. 405–421, 2021.

- [4] W. Kool, H. van Hoof, and M. Welling, "Attention, learn to solve routing problems!" in *International Conference on Learning Representations*, 2019.
- [5] A. Bogrybayeva, M. Meraliyev, T. Mustakhov, and B. Dauletbayev, "Machine learning to solve vehicle routing problems: A survey," *IEEE Transactions on Intelligent Transportation Systems*, 2024.
- [6] Y.-D. Kwon, J. Choo, B. Kim, I. Yoon, Y. Gwon, and S. Min, "Pomo: Policy optimization with multiple optima for reinforcement learning," *Advances in Neural Information Processing Systems*, vol. 33, pp. 21 188–21 198, 2020.
- [7] I. Drori, A. Kharkar, W. R. Sickinger, B. Kates, Q. Ma, S. Ge, E. Dolev, B. Dietrich, D. P. Williamson, and M. Udell, "Learning to solve combinatorial optimization problems on real-world graphs in linear time," in *2020 19th IEEE International Conference on Machine Learning and Applications (ICMLA)*. IEEE, 2020, pp. 19–24.
- [8] L. Duan, Y. Zhan, H. Hu, Y. Gong, J. Wei, X. Zhang, and Y. Xu, "Efficiently solving the practical vehicle routing problem: A novel joint learning approach," in *Proceedings of the 26th ACM SIGKDD international conference on knowledge discovery & data mining*, 2020, pp. 3054–3063.
- [9] L. Gao, M. Chen, Q. Chen, G. Luo, N. Zhu, and Z. Liu, "Learn to design the heuristics for vehicle routing problem," *arXiv preprint arXiv:2002.08539*, 2020.
- [10] Q. Cappart, T. Moisan, L.-M. Rousseau, I. Prémont-Schwarz, and A. A. Cire, "Combining reinforcement learning and constraint programming for combinatorial optimization," in *Proceedings of the AAAI Conference on Artificial Intelligence*, vol. 35, no. 5, 2021, pp. 3677–3687.
- [11] J. Zhao, M. Mao, X. Zhao, and J. Zou, "A hybrid of deep reinforcement learning and local search for the vehicle routing problems," *IEEE Transactions on Intelligent Transportation Systems*, vol. 22, no. 11, pp. 7208–7218, 2021.
- [12] W. Kool, H. van Hoof, J. Gromicho, and M. Welling, "Deep policy dynamic programming for vehicle routing problems," in *International conference on integration of constraint programming, artificial intelligence, and operations research*. Springer, 2022, pp. 190–213.
- [13] R. Tyasnurita, E. Özcan, and R. John, "Learning heuristic selection using a time delay neural network for open vehicle routing," in *2017 IEEE Congress on Evolutionary Computation (CEC)*. Ieee, 2017, pp. 1474–1481.
- [14] S.-Y. Tan and W.-C. Yeh, "The vehicle routing problem: State-of-the-art classification and review," *Applied Sciences*, vol. 11, no. 21, 2021. [Online]. Available: <https://www.mdpi.com/2076-3417/11/21/10295>
- [15] F. Liu, X. Lin, Z. Wang, Q. Zhang, X. Tong, and Y. Mingxuan, "Multi-task learning for routing problem with cross-problem zero-shot generalization," in *The 30th ACM SIGKDD Conference on Knowledge Discovery and Data Mining (KDD 2024)*. Association for Computing Machinery, 2024.
- [16] J. Zhou, Z. Cao, Y. Wu, W. Song, Y. Ma, J. Zhang, and C. Xu, "Mvmoe: Multi-task vehicle routing solver with mixture-of-experts," in *International Conference on Machine Learning (ICML)*, 2024.
- [17] F. Berto, C. Hua, N. G. Zepeda, A. Hottung, N. Wouda, L. Lan, K. Tierney, and J. Park, "Routerfinder: Towards foundation models for vehicle routing problems," in *ICML 2024 Workshop on Foundation Models in the Wild*, 2024, <https://github.com/ai4co/routerfinder>. [Online]. Available: <https://openreview.net/forum?id=hCiaiz6e4G>
- [18] Z. Lin, Y. Wu, B. Zhou, Z. Cao, W. Song, Y. Zhang, and J. Senthilnath, "Cross-problem learning for solving vehicle routing problems," in *The 33rd International Joint Conference on Artificial Intelligence (IJCAI-24)*, 2024.
- [19] N. Shazeer, A. Mirhoseini, K. Maziarz, A. Davis, Q. Le, G. Hinton, and J. Dean, "Outrageously large neural networks: The sparsely-gated mixture-of-experts layer," in *International Conference on Learning Representations*, 2017.
- [20] A. Dubey, A. Jauhri, A. Pandey, A. Kadian, A. Al-Dahle, A. Letman, A. Mathur, A. Schelten, A. Yang, A. Fan *et al.*, "The llama 3 herd of models," *arXiv preprint arXiv:2407.21783*, 2024.
- [21] X. Chen, H. Li, M. Li, and J. Pan, "Learning a sparse transformer network for effective image deraining," in *Proceedings of the IEEE/CVF Conference on Computer Vision and Pattern Recognition*, 2023, pp. 5896–5905.
- [22] S. Zhou, D. Chen, J. Pan, J. Shi, and J. Yang, "Adapt or perish: Adaptive sparse transformer with attentive feature refinement for image restoration," in *Proceedings of the IEEE/CVF Conference on Computer Vision and Pattern Recognition*, 2024, pp. 2952–2963.
- [23] M. Nazari, A. Oroojlooy, L. Snyder, and M. Takác, "Reinforcement learning for solving the vehicle routing problem," *Advances in neural information processing systems*, vol. 31, 2018.
- [24] O. Vinyals, M. Fortunato, and N. Jaitly, "Pointer networks," *Advances in neural information processing systems*, vol. 28, 2015.
- [25] R. J. Williams, "Simple statistical gradient-following algorithms for connectionist reinforcement learning," *Machine learning*, vol. 8, pp. 229–256, 1992.
- [26] L. Xin, W. Song, Z. Cao, and J. Zhang, "Multi-decoder attention model with embedding glimpse for solving vehicle routing problems," in *Proceedings of the AAAI Conference on Artificial Intelligence*, vol. 35, no. 13, 2021, pp. 12 042–12 049.
- [27] M. Kim, J. Park *et al.*, "Learning collaborative policies to solve np-hard routing problems," *Advances in Neural Information Processing Systems*, vol. 34, pp. 10 418–10 430, 2021.
- [28] B. Peng, J. Wang, and Z. Zhang, "A deep reinforcement learning algorithm using dynamic attention model for vehicle routing problems," in *Artificial Intelligence Algorithms and Applications: 11th International Symposium, ISICA 2019, Guangzhou, China, November 16–17, 2019, Revised Selected Papers 11*. Springer, 2020, pp. 636–650.
- [29] M. Kim, J. Park, and J. Park, "Sym-nco: Leveraging symmetricity for neural combinatorial optimization," *Advances in Neural Information Processing Systems*, vol. 35, pp. 1936–1949, 2022.
- [30] J. Li, Y. Ma, R. Gao, Z. Cao, A. Lim, W. Song, and J. Zhang, "Deep reinforcement learning for solving the heterogeneous capacitated vehicle routing problem," *IEEE Transactions on Cybernetics*, vol. 52, no. 12, pp. 13 572–13 585, 2022.
- [31] A. Bogrybayeva, M. Meraliyev, T. Mustakhov, and B. Dauletbayev, "Learning to solve vehicle routing problems: A survey," *arXiv preprint arXiv:2205.02453*, 2022.
- [32] B. Li, G. Wu, Y. He, M. Fan, and W. Pedrycz, "An overview and experimental study of learning-based optimization algorithms for the vehicle routing problem," *IEEE/CAA Journal of Automatica Sinica*, vol. 9, no. 7, pp. 1115–1138, 2022.
- [33] Z. Zhang, Z. Zhang, X. Wang, and W. Zhu, "Learning to solve travelling salesman problem with hardness-adaptive curriculum," in *Proceedings of the AAAI Conference on Artificial Intelligence*, vol. 36, no. 8, 2022, pp. 9136–9144.
- [34] L. Xin, W. Song, Z. Cao, and J. Zhang, "Generative adversarial training for neural combinatorial optimization models," 2022. [Online]. Available: <https://openreview.net/forum?id=9vsRT9mc7U>
- [35] S. Geisler, J. Sommer, J. Schuchardt, A. Bojchevski, and S. Günnemann, "Generalization of neural combinatorial solvers through the lens of adversarial robustness," in *International Conference on Learning Representations*, 2022.
- [36] C. Wang, Y. Yang, C. Han, T. Guo, H. Zhang, and J. Wang, "A game-theoretic approach for improving generalization ability of tsp solvers," in *ICLR 2022 Workshop on Gamification and Multiagent Solutions*, 2022.
- [37] Y. Jiang, Y. Wu, Z. Cao, and J. Zhang, "Learning to solve routing problems via distributionally robust optimization," in *Proceedings of the AAAI Conference on Artificial Intelligence*, vol. 36, no. 9, 2022, pp. 9786–9794.
- [38] J. Bi, Y. Ma, J. Wang, Z. Cao, J. Chen, Y. Sun, and Y. M. Chee, "Learning generalizable models for vehicle routing problems via knowledge distillation," *Advances in Neural Information Processing Systems*, vol. 35, pp. 31 226–31 238, 2022.
- [39] J. Zhou, Y. Wu, W. Song, Z. Cao, and J. Zhang, "Towards omnigeneralizable neural methods for vehicle routing problems," in *International Conference on Machine Learning*. PMLR, 2023, pp. 42 769–42 789.
- [40] C. Wang and T. Yu, "Efficient training of multi-task neural solver with multi-armed bandits," *arXiv preprint arXiv:2305.06361*, 2023.
- [41] Y. N. Dauphin, A. Fan, M. Auli, and D. Grangier, "Language modeling with gated convolutional networks," in *International conference on machine learning*. PMLR, 2017, pp. 933–941.
- [42] B. Zhang and R. Sennrich, "Root mean square layer normalization," *Advances in Neural Information Processing Systems*, vol. 32, 2019.
- [43] A. Baevski and M. Auli, "Adaptive input representations for neural language modeling," *arXiv preprint arXiv:1809.10853*, 2018.
- [44] R. Child, S. Gray, A. Radford, and I. Sutskever, "Generating long sequences with sparse transformers," *arXiv preprint arXiv:1904.10509*, 2019.
- [45] O. Ronneberger, P. Fischer, and T. Brox, "U-net: Convolutional networks for biomedical image segmentation," in *Medical image computing and*

- computer-assisted intervention—MICCAI 2015: 18th international conference, Munich, Germany, October 5-9, 2015, proceedings, part III 18. Springer, 2015, pp. 234–241.
- [46] M.-H. Guo, C.-Z. Lu, Q. Hou, Z. Liu, M.-M. Cheng, and S.-M. Hu, “Segnext: Rethinking convolutional attention design for semantic segmentation,” *Advances in Neural Information Processing Systems*, vol. 35, pp. 1140–1156, 2022.
- [47] J. Gu, H. Kwon, D. Wang, W. Ye, M. Li, Y.-H. Chen, L. Lai, V. Chandra, and D. Z. Pan, “Multi-scale high-resolution vision transformer for semantic segmentation,” in *Proceedings of the IEEE/CVF conference on computer vision and pattern recognition*, 2022, pp. 12 094–12 103.
- [48] K. Sun, Y. Zhao, B. Jiang, T. Cheng, B. Xiao, D. Liu, Y. Mu, X. Wang, W. Liu, and J. Wang, “High-resolution representations for labeling pixels and regions,” *arXiv preprint arXiv:1904.04514*, 2019.
- [49] J. Wang, K. Sun, T. Cheng, B. Jiang, C. Deng, Y. Zhao, D. Liu, Y. Mu, M. Tan, X. Wang *et al.*, “Deep high-resolution representation learning for visual recognition,” *IEEE transactions on pattern analysis and machine intelligence*, vol. 43, no. 10, pp. 3349–3364, 2020.
- [50] J. Fu, J. Liu, H. Tian, Y. Li, Y. Bao, Z. Fang, and H. Lu, “Dual attention network for scene segmentation,” in *Proceedings of the IEEE/CVF conference on computer vision and pattern recognition*, 2019, pp. 3146–3154.
- [51] J. Zhang, Z. Tu, J. Yang, Y. Chen, and J. Yuan, “Mixste: Seq2seq mixed spatio-temporal encoder for 3d human pose estimation in video,” in *Proceedings of the IEEE/CVF conference on computer vision and pattern recognition*, 2022, pp. 13 232–13 242.
- [52] X. Dong, J. Bao, D. Chen, W. Zhang, N. Yu, L. Yuan, D. Chen, and B. Guo, “Cswin transformer: A general vision transformer backbone with cross-shaped windows,” in *Proceedings of the IEEE/CVF conference on computer vision and pattern recognition*, 2022, pp. 12 124–12 134.
- [53] W. Wang, W. Chen, Q. Qiu, L. Chen, B. Wu, B. Lin, X. He, and W. Liu, “Crossformer++: A versatile vision transformer hinging on cross-scale attention,” *IEEE Transactions on Pattern Analysis and Machine Intelligence*, 2023.
- [54] H. Zhang, K. Dana, J. Shi, Z. Zhang, X. Wang, A. Tyagi, and A. Agrawal, “Context encoding for semantic segmentation,” in *Proceedings of the IEEE conference on Computer Vision and Pattern Recognition*, 2018, pp. 7151–7160.
- [55] G. Zhao, J. Lin, Z. Zhang, X. Ren, Q. Su, and X. Sun, “Explicit sparse transformer: Concentrated attention through explicit selection,” *arXiv preprint arXiv:1912.11637*, 2019.
- [56] P. Wang, X. Wang, F. Wang, M. Lin, S. Chang, H. Li, and R. Jin, “Kvt: k-nn attention for boosting vision transformers,” in *European conference on computer vision*. Springer, 2022, pp. 285–302.
- [57] H. Wang, J. Shen, Y. Liu, Y. Gao, and E. Gavves, “Nformer: Robust person re-identification with neighbor transformer,” in *Proceedings of the IEEE/CVF conference on computer vision and pattern recognition*, 2022, pp. 7297–7307.
- [58] H. Zhao, Y. Gou, B. Li, D. Peng, J. Lv, and X. Peng, “Comprehensive and delicate: An efficient transformer for image restoration,” in *Proceedings of the IEEE/CVF conference on computer vision and pattern recognition*, 2023, pp. 14 122–14 132.
- [59] Q. Guo, X. Qiu, P. Liu, Y. Shao, X. Xue, and Z. Zhang, “Star-transformer,” *arXiv preprint arXiv:1902.09113*, 2019.
- [60] S. Li, X. Jin, Y. Xuan, X. Zhou, W. Chen, Y.-X. Wang, and X. Yan, “Enhancing the locality and breaking the memory bottleneck of transformer on time series forecasting,” *Advances in neural information processing systems*, vol. 32, 2019.
- [61] I. Beltagy, M. E. Peters, and A. Cohan, “Longformer: The long-document transformer,” *arXiv preprint arXiv:2004.05150*, 2020.
- [62] J. Ainslie, S. Ontanon, C. Alberti, V. Cvicek, Z. Fisher, P. Pham, A. Ravula, S. Sanghai, Q. Wang, and L. Yang, “Etc: Encoding long and structured inputs in transformers,” *arXiv preprint arXiv:2004.08483*, 2020.
- [63] A. Martins and R. Astudillo, “From softmax to sparsemax: A sparse model of attention and multi-label classification,” in *International conference on machine learning*. PMLR, 2016, pp. 1614–1623.
- [64] B. Peters, V. Niculae, and A. F. Martins, “Sparse sequence-to-sequence models,” pp. 1504–1519, 2019.
- [65] M. Blondel, A. Martins, and V. Niculae, “Learning classifiers with fenchel-young losses: Generalized entropies, margins, and algorithms,” in *The 22nd International Conference on Artificial Intelligence and Statistics*. PMLR, 2019, pp. 606–615.
- [66] G. M. Correia, V. Niculae, and A. F. Martins, “Adaptively sparse transformers,” in *Proceedings of the 2019 Conference on Empirical Methods in Natural Language Processing and the 9th International Joint Conference on Natural Language Processing (EMNLP-IJCNLP)*, 2019, pp. 2174–2184.
- [67] A. Vaswani, N. Shazeer, N. Parmar, J. Uszkoreit, L. Jones, A. N. Gomez, L. Kaiser, and I. Polosukhin, “Attention is all you need,” *Advances in neural information processing systems*, vol. 30, 2017.
- [68] A. Chowdhery, S. Narang, J. Devlin, M. Bosma, G. Mishra, A. Roberts, P. Barham, H. W. Chung, C. Sutton, S. Gehrmann *et al.*, “Palm: Scaling language modeling with pathways,” *Journal of Machine Learning Research*, vol. 24, no. 240, pp. 1–113, 2023.
- [69] H. Touvron, T. Lavril, G. Izacard, X. Martinet, M.-A. Lachaux, T. Lacroix, B. Rozière, N. Goyal, E. Hambro, F. Azhar *et al.*, “Llama: Open and efficient foundation language models,” *arXiv preprint arXiv:2302.13971*, 2023.
- [70] H. Naveed, A. U. Khan, S. Qiu, M. Saqib, S. Anwar, M. Usman, N. Akhtar, N. Barnes, and A. Mian, “A comprehensive overview of large language models,” *arXiv preprint arXiv:2307.06435*, 2023.
- [71] S. Elfving, E. Uchibe, and K. Doya, “Sigmoid-weighted linear units for neural network function approximation in reinforcement learning,” *Neural networks*, vol. 107, pp. 3–11, 2018.
- [72] N. Shazeer, “Glu variants improve transformer,” *arXiv preprint arXiv:2002.05202*, 2020.
- [73] K. He, X. Zhang, S. Ren, and J. Sun, “Deep residual learning for image recognition,” in *Proceedings of the IEEE conference on computer vision and pattern recognition*, 2016, pp. 770–778.
- [74] I. Loshchilov, “Decoupled weight decay regularization,” *arXiv preprint arXiv:1711.05101*, 2017.
- [75] N. A. Wouda, L. Lan, and W. Kool, “Pyvrp: A high-performance vrp solver package,” *INFORMS Journal on Computing*, 2024.
- [76] T. Vidal, “Hybrid genetic search for the cvrp: Open-source implementation and swap* neighborhood,” *Computers & Operations Research*, vol. 140, p. 105643, 2022.
- [77] E. Uchoa, D. Pecin, A. Pessoa, M. Poggi, T. Vidal, and A. Subramanian, “New benchmark instances for the capacitated vehicle routing problem,” *European Journal of Operational Research*, vol. 257, no. 3, pp. 845–858, 2017.